Bioconjugate Chemistry

Article

pubs.acs.org/bc

Novel ^{99m}Tc(III) Complexes [^{99m}TcCl(CDO)(CDOH)$_2$B−R] (CDOH$_2$ = Cyclohexanedione Dioxime) Useful as Radiotracers for Heart Imaging

Min Liu,[†,‡] Wei Fang,[*,§] and Shuang Liu[*,‡]

[†]Department of Radiation Medicine and Protection, Medical College, Soochow University, China

[‡]School of Health Sciences, Purdue University, Indiana 47907, United States

[§]Department of Nuclear Medicine, Fuwai Hospital, the National Center for Cardiovascular Diseases, Chinese Academy of Medical Sciences and Peking Union Medical College, Beijing, China

Supporting Information

ABSTRACT: In this study, we evaluated seven new ^{99m}Tc(III) complexes [^{99m}TcCl(CDO)(CDOH)$_2$B−R] (^{99m}Tc−2Fboroxime: R = 2-formylfuran-3-yl (2F); ^{99m}Tc−3Fboroxime: R = furan-3-yl (3F); ^{99m}Tc−5Fboroxime: R = 5-formyfuran-2-yl (5F); ^{99m}Tc−HPboroxime: R = 6-hydroxylpyridin-2-yl (HP); ^{99m}Tc−MPYboroxime: R = 5-methoxypyridin-3-yl (MPY); ^{99m}Tc−PMboroxime: R = 1,5-pyrimidin-3-yl (PM); and ^{99m}Tc−4PYboroxime: R = pyridin-4-yl (4PY)) for their potential as heart imaging agents. All new ^{99m}Tc(III) radiotracers except ^{99m}Tc−2Fboroxime were prepared with high radiochemical purity (RCP > 95%). The low RCP (~75%) for ^{99m}Tc−2Fboroxime is most likely caused by steric hindrance from the 3-formyl group. Biodistribution and imaging studies were performed in SD rats. Planar image quantification was performed to compare their myocardial retention times. We found that the myocardial washout curves of new ^{99m}Tc(III) radiotracers were best fitted the biexponential decay function. The AUC (area under the curve) values followed the general trend: ^{99m}Tc−5Fboroxime (129 ± 6) > ^{99m}Tc−3Fboroxime (114 ± 11) > ^{99m}Tc−Teboroxime (104 ± 16) > ^{99m}Tc−MPYboroxime (92 ± 18) > ^{99m}Tc−4PYboroxime (77 ± 10) > ^{99m}Tc−PMboroxime (68 ± 14) ≈ ^{99m}Tc−HPboroxime (62 ± 14). The 2 min heart uptake values from biodistribution studies follow the ranking order of ^{99m}Tc−5Fboroxime (3.75 ± 0.15%ID/g) ≈ ^{99m}Tc−MPYboroxime (3.73 ± 0.24%ID/g) > ^{99m}Tc−PMboroxime (3.47 ± 0.15%ID/g) ≈ ^{99m}Tc−3Fboroxime ≈ (3.25 ± 0.77%ID/g). The 5 min heart uptake of ^{99m}Tc−5Fboroxime (3.91 ± 0.09%ID/g) was almost identical to its 2 min heart uptake (3.75 ± 0.15%ID/g), and its 15 min heart uptake value (2.83 ± 0.08%ID/g) compared well to the 2 min heart uptake of ^{99m}Tc−Teboroxime (3.00 ± 0.37%ID/g). It took ~5 min for ^{99m}Tc−5Fboroxime to approach the 1 min heart uptake value of ^{99m}Tc−Teboroxime (~3.5% ID/g) and ~9.5 min to reach the 2 min heart uptake value of ^{99m}Tc−Teboroxime (~3.0% ID/g). The best image acquisition window is 0−5 min for ^{99m}Tc−5Fboroxime. High-quality single-photon emission computed tomography images of the rat hearts were acquired in any of the 5 min window over the first 20 min after its administration. ^{99m}Tc−5Fboroxime has significant advantages over ^{99m}Tc−Teboroxime as the radiotracer for myocardial perfusion imaging.

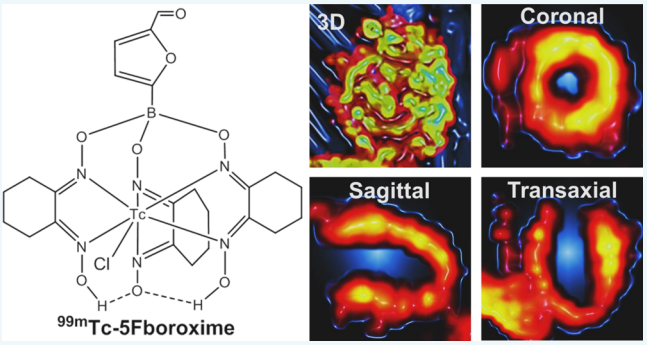

INTRODUCTION

More than 70 million Americans live with cardiovascular diseases (CAD), which are the leading cause of premature death and permanent disability. CAD arises from gradual narrowing of coronary artery due to atherosclerotic deposits. The progressive narrowing of coronary artery eventually predisposes the patient to myocardial ischemia, a serious condition in which the coronary blood flow decreases to a level below what is needed to meet the demand for oxygen and nutrients. In the advanced CAD, the blood flow and tissue oxygen are too low to sustain cardiac function at rest, leading to myocardial infarction. Thus, accurate early detection of CAD is highly desirable so that appropriate therapeutic regimens can be given before irreversible damage occurs in the patients with known or suspected CAD.

Myocardial perfusion imaging (MPI) with radiotracers is a noninvasive technique showing the heart function and the areas of heart muscle with perfusion defects and remains an integral component in evaluation of CAD patients.[1−6] If the patient has CAD, there will be perfusion defects in the heart in response to the reduced blood flow. If the reduced uptake is worse under stress conditions than at rest, the perfusion defect is likely caused by myocardial ischemia. If the reduced uptake is the same under rest and stress conditions, the perfusion defect is likely caused by myocardial infarction. To evaluate the area of perfusion defect with accuracy, the radiotracer must be taken

Received: September 22, 2016
Revised: October 12, 2016
Published: October 13, 2016

DOI: 10.1021/acs.bioconjchem.6b00552
Bioconjugate Chem. 2016, 27, 2770−2779

up into myocardium in proportion to the regional blood flow. Precise measurement of blood flow is of great clinical importance in identifying ischemia, defining the extent and severity of disease, assessing myocardial viability, establishing the need for surgical intervention, and monitoring the effects of treatment in CAD patients. ^{99m}Tc−Sestamibi is the most widely used radiotracer for MPI in nuclear cardiology. A significant drawback of ^{99m}Tc−Sestamibi is its low first-pass extraction fraction and lack of linear relationship between its heart uptake and regional blood flow rates at >2.5 mL/min/g.[3,7] In contrast, ^{99m}Tc−Teboroxime ([^{99m}TcCl(CDO)(CDOH)$_2$B−Me]: $CDOH_2$ = cyclohexanedione dioxime) has the highest first-pass extraction fraction among all ^{99m}Tc radiotracers.[11−15] However, its early clinical experiences with were disappointing because of its short myocardial retention.[16,17] More than 60% of its initial heart activity is washed out within 5 min post-injection (p.i.).[3,7,16,17] The uptake-flow relationship was linear only up to 2.5 mL/min/g at 5 min after administration, which makes it hard to accurately quantify the heart activity. With the developments in the cadmium zinc telluride (CZT)-based single-photon emission computed tomography (SPECT) cameras,[18−29] the leaders in nuclear cardiology have been calling for more efficient perfusion radiotracers with longer myocardial retention, improved biodistribution properties, or both.[3,30−34]

We have been interested in ^{99m}Tc(III) complexes [^{99m}TcL-(CDO)(CDOH)$_2$B−R] (L = Cl, F, N_3 and SCN; R = alkyls or aryls) as radiotracers for MPI[35−37] because ^{99m}Tc−Teboroxime has a high first-pass extraction fraction and shows the linear relationship between its heart uptake and the regional blood flow rate up to 5 mL/min/g at 1−2 min p.i.[15] In this report, we present the evaluation of complexes [^{99m}TcCl(CDO)-(CDOH)$_2$B−R] (Figure 1: R = 2F, 3F, 5F, HP, MPY, PM, and 4PY) for their potential as radiotracers for heart imaging. We kept the $CDOH_2$ core to maintain their high initial heart uptake. Different boronate caps were used to balance their lipophilicity, initial heart uptake, and myocardial retention time. The main objective of this study was to develop a ^{99m}Tc radiotracer with longer myocardial retention than that of ^{99m}Tc−Terboroxime while maintaining the high first-pass extraction fraction. A more stable heart uptake and longer myocardial retention will help to maintain the linear relationship between the radiotracer heart uptake and blood flow.[15] The combination of high heart uptake and long myocardial retention will make it possible to use the new radiotracer for MPI studies with both standard and CZT-based ultrafast cardiac SPECT cameras.

RESULTS

Radiochemistry. All new ^{99m}Tc(III) complexes [^{99m}TcCl-(CDO)(CDOH)$_2$B−R] (R = 2F, 3F, 5F, HP, MPY, PM, and 4PY) were prepared according to Chart 1 using the kit formulation.[35−37] Table 1 lists radiochemical purity (RCP) data and HPLC retention times of ^{99m}Tc−Teboroxime and new ^{99m}Tc(III) radiotracers [^{99m}TcCl(CDO)(CDOH)$_2$B−R] (R = 2F, 3F, 5F, HP, MPY, PM, and 4PY). The RCP values were 95−98% for new radiotracers [^{99m}TcCl(CDO)(CDOH)$_2$B−R] (R = 3F, 5F, HP, MPY, PM, and 4PY), with the radioimpurity being <2% (Figure SI1). The RCP for ^{99m}Tc−2Fboroxime was ∼75% due to the radioimpurity at ∼9 min in its HPLC chromatogram (Figure SI1). The steric effect from the 3-formyl group may force part of ^{99m}Tc−2Fboroxime (Figure 1) to adopt the partially capped binding mode, in which only two of three dioxime O atoms are bonded by the boronate cap. Partial capping is well-documented in the tris(dioxime) complexes of Mn(II) and Re(III).[38,39] Complexes [^{99m}TcCl(CDO)-(CDOH)$_2$B−R] (R = 3F, 5F, HP, MPY, PM, and 4PY) were stable for >6 h at room temperature, both in the kit matrix and in the diluted saline solution containing 20−30% propylene glycol.

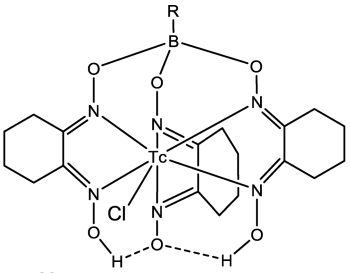

[^{99m}TcCl(CDO)(CDOH)B-R]

^{99m}Tc(III) Complex	Radiotracer	R Group
[^{99m}TcCl(CDO)(CDOH)B-Me]	^{99m}Tc-Teboroxime	CH_3
[^{99m}TcCl(CDO)(CDOH)B-IS]	^{99m}Tc-ISboroxime	
[^{99m}TcCl(CDO)(CDOH)B-PA]	^{99m}Tc-PAboroxime	
[^{99m}TcCl(CDO)(CDOH)B-2F]	^{99m}Tc-2Fboroxime	
[^{99m}TcCl(CDO)(CDOH)B-3F]	^{99m}Tc-3Fboroxime	
[^{99m}TcCl(CDO)(CDOH)B-5F]	^{99m}Tc-5Fboroxime	
[^{99m}TcCl(CDO)(CDOH)B-HP]	^{99m}Tc-HPboroxime	
[^{99m}TcCl(CDO)(CDOH)B-MPY]	^{99m}Tc-MPYboroxime	
[^{99m}TcCl(CDO)(CDOH)B-PM]	^{99m}Tc-PMboroxime	
[^{99m}TcCl(CDO)(CDOH)B-4PY]	^{99m}Tc-4PYboroxime	

Figure 1. Chemdraw structures of ^{99m}Tc(III) complexes [^{99m}TcCl-(CDO)(CDOH)$_2$B−R]. ^{99m}Tc−Teboroxime is a well-known radiotracer for myocardial perfusion imaging in nuclear cardiology. ^{99m}Tc−ISboroxime and ^{99m}Tc−PAboroxime have been evaluated in our previous reports.[36] New ^{99m}Tc(III) complexes [^{99m}TcCl(CDO)-(CDOH)$_2$B−R] (R = 2F, 3F, 5F, HP, MPY, PM, and 4PY) were evaluated in this study for their potential as new heart-imaging agents.

Chart 1. Synthesis of New ^{99m}Tc(III) Complexes [^{99m}TcCl(CDO)(CDOH)$_2$B−R] (R = 2F, 3F, 5F, HP, MPY, PM, and 4PY)

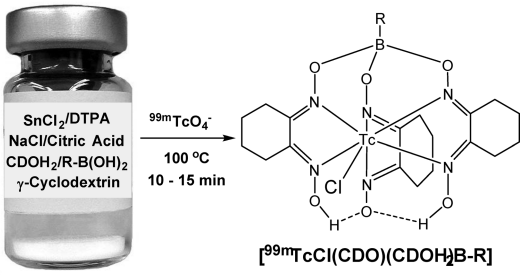

[^{99m}TcCl(CDO)(CDOH)$_2$B-R]

Dynamic Planar Imaging. Planar imaging was used as a screening tool to evaluate the heart washout kinetics of ^{99m}Tc radiotracers without sacrificing a large number of animals. We

DOI: 10.1021/acs.bioconjchem.6b00552
Bioconjugate Chem. 2016, 27, 2770−2779

Table 1. Radiochemical Purity Data and HPLC Retention Times of ^{99m}Tc−Teboroxime and New ^{99m}Tc(III) Radiotracers [^{99m}TcCl(CDO)(CDOH)$_2$B−R] (R = 2F, 3F, 5F, HP, MPY, PM, and 4PY)

^{99m}Tc(III) complex	radiotracer (abbreviation)	HPLC retention time (min)	radiochemical purity (%)
[^{99m}TcCl(CDO)(CDOH)B−Me]	^{99m}Tc−Teboroxime	15.5	>95%
[^{99m}TcCl(CDO)(CDOH)B−2F]	^{99m}Tc−2Fboroxime	13.2	∼75%
[^{99m}TcCl(CDO)(CDOH)B−3F]	^{99m}Tc−3Fboroxime	16.5	>95%
[^{99m}TcCl(CDO)(CDOH)B−5F]	^{99m}Tc−5Fboroxime	11.2	>95%
[^{99m}TcCl(CDO)(CDOH)B−HP]	^{99m}Tc−HPboroxime	7.2	>95%
[^{99m}TcCl(CDO)(CDOH)B−MPY]	^{99m}Tc−MPYboroxime	15.3	>95%
[^{99m}TcCl(CDO)(CDOH)B−PM]	^{99m}Tc−PMboroxime	11.8	>95%
[^{99m}TcCl(CDO)(CDOH)B−4PY]	^{99m}Tc−4PYboroxime	14.2	>95%

carried out planar imaging studies on ^{99m}Tc(III) complexes [^{99m}TcCl(CDO)(CDOH)$_2$B−R] (R = 3F, 5F, HP, MPY, PM, and 4PY). ^{99m}Tc−2Fboroxime was excluded because of its low RCP (Figure S1). There are two important parameters in planar imaging with ^{99m}Tc radiotracers: the initial heart uptake and area under the curve (AUC) values. Table 2 lists the image quantification data used to compare their initial heart uptake and AUC values. Among the new ^{99m}Tc(III) radiotracers evaluated in planar imaging studies, ^{99m}Tc−HPboroxime had the lowest the initial heart uptake, and the remaining five new ^{99m}Tc(III) radiotracers shared similar initial heart uptake values (Table 2). Their myocardial washout curves best fit the biexponential decay function. Figure 2A shows typical planar images for the SD rats administered with ^{99m}Tc−5Fboroxime and ^{99m}Tc−Teboroxime. Figure 2B compares their myocardial washout kinetics. The AUC values calculated according to their respective biexponential equations followed the general ranking order of ^{99m}Tc−5Fboroxime > ^{99m}Tc−3Fboroxime > ^{99m}Tc−Teboroxime > ^{99m}Tc−MPYboroxime > ^{99m}Tc−4PYboroxime ∼ ^{99m}Tc−PMboroxime > ^{99m}Tc−HPboroxime. The heart uptake values of ^{99m}Tc−5Fboroxime were significantly higher than that of ^{99m}Tc−Teboroxime at >2 min after administration (Figure 3B), suggesting that ^{99m}Tc−5Fboroxime has the advantage over ^{99m}Tc−Teboroxime.

Table 2. Planar Image Quantification Data Used to Compare the Initial Heart Uptake and AUC Values of New ^{99m}Tc(III) Radiotracers[a]

radiotracer	initial heart uptake (% ID)	AUC (0−60 min)	R^2
^{99m}Tc−Teboroxime	4.6 ± 0.9	104 ± 16	0.9914
^{99m}Tc−3Fboroxime	5.7 ± 0.6	114 ± 11	0.9915
^{99m}Tc−5Fboroxime	5.1 ± 0.9	129 ± 6	0.9923
^{99m}Tc−HPboroxime	3.2 ± 0.7	62 ± 14	0.9954
^{99m}Tc−MPYboroxime	4.4 ± 0.6	92 ± 18	0.9951
^{99m}Tc−PMboroxime	5.3 ± 0.1	68 ± 14	0.9932
^{99m}Tc−4PYboroxime	5.7 ± 0.4	77 ± 10	0.9703

[a]Their initial heart uptake (the % ID heart uptake at 1 min post-injection) and AUC values were calculated as according to their respective bi-exponential decay equations.

Comparison of 2 min Heart Uptake. We performed the 2 min biodistribution on four new ^{99m}Tc(III) radiotracers (^{99m}Tc−3Fboroxime, ^{99m}Tc−5Fboroxime, ^{99m}Tc−PMboroxime, and ^{99m}Tc−MPYboroxime), all of which have the initial heart uptake (Table 2) equivalent to or better than those of ^{99m}Tc−Teboroxime. ^{99m}Tc−4PYboroxime was excluded because of its fast myocardial washout. ^{99m}Tc−HPboroxime was not used due to its low initial heart uptake (Table 2). ^{99m}Tc−Teboroxime and ^{99m}Tc−Sestamibi were evaluated in the same model for comparison purposes. Table 3 lists their 2 min heart uptake values, which follow the order of ^{99m}Tc−5Fboroxime ∼ ^{99m}Tc−MPYboroxime ∼ ^{99m}Tc−3Fboroxime > ^{99m}Tc−PMboroxime ∼ ^{99m}Tc−Teboroxime. The % ID heart uptake values of ^{99m}Tc−Teboroxime and its derivatives were significantly higher ($p < 0.01$) than that of ^{99m}Tc−Sestamibi; however, these values were significantly lower ($p < 0.01$) than that reported for ^{99m}Tc−Teboroxime (3.4% ID in SD rats of 100−125 g).[11,15] This could be caused by the differences in the cardiac output, the fractional cardiac output to the myocardium, or both. The younger rats tend to have higher blood flow rate into the myocardium than older rats.[11,12]

Table 4 lists the selected 2 min biodistribution data of ^{99m}Tc−3Fboroxime, ^{99m}Tc−5Fboroxime, ^{99m}Tc−MPYborox-

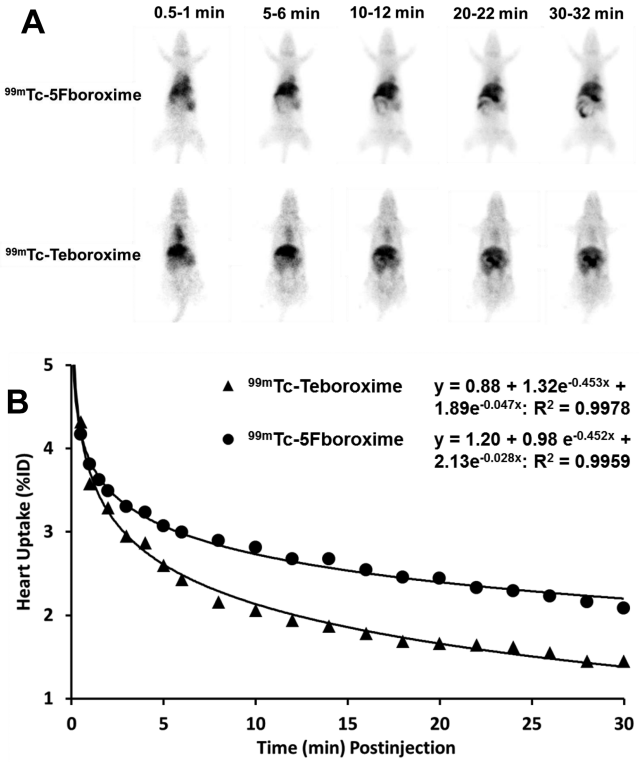

Figure 2. (A) Dynamic planar images of the SD rats administered with ^{99m}Tc−5Fboroxime and ^{99m}Tc−Teboroxime. (B) Comparison of myocardial washout kinetics of ^{99m}Tc−5Fboroxime and ^{99m}Tc−Teboroxime. All experimental data were from planar image quantification in five SD rats. Standard error bars were omitted for its clarity.

DOI: 10.1021/acs.bioconjchem.6b00552
Bioconjugate Chem. 2016, 27, 2770−2779

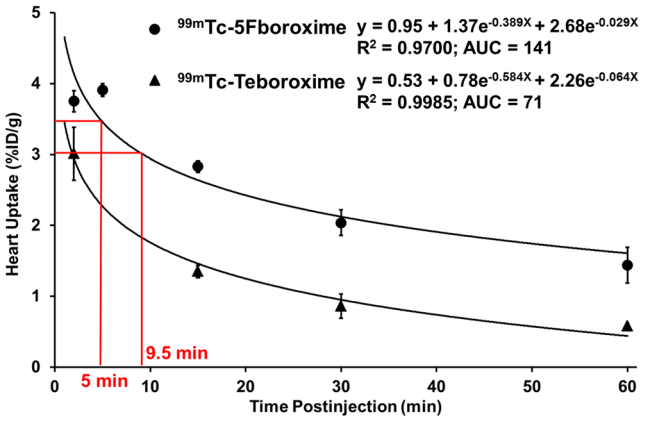

Radiotracer	^{99m}Tc-Teboroxime	^{99m}Tc-5Fboroxime
AUC at 0 – 5 min	15.04	21.01
AUC at 0 – 10 min	24.98	36.86
AUC at 0 – 15 min	32.99	50.76
AUC at 0 – 30 min	50.67	86.03
AUC at 0 – 60 min	70.73	141.09

Figure 3. Comparison of myocardial washout kinetics of ^{99m}Tc–5Fboroxime and ^{99m}Tc–Teboroxime. All experimental data were from biodistribution studies in SD rats (n = 3–4). It took ~5 min for ^{99m}Tc–5Fboroxime to approach the 1 min heart uptake value (3.5% ID/g) and ~9.5 min to reach the 2 min heart uptake value (3.05% ID/g) of ^{99m}Tc–Teboroxime. The AUC value for ^{99m}Tc–5Fboroxime was almost twice of that for ^{99m}Tc–Teboroxime at 0–60 min.

Table 3. Percentage of the Injected Dose (% ID) at 2 min Post-injection for ^{99m}Tc–3Fboroxime, ^{99m}Tc–5Fboroxime, ^{99m}Tc–MPYboroxime, and ^{99m}Tc–PMboroxime in the Myocardium of SD Rats (200 ± 225 g) in Comparison to Those of ^{99m}Tc–Sestamibi and ^{99m}Tc–Teboroxime

radiotracer	total heart uptake (% ID) at 2 min post-injection[a]
^{99m}Tc–Sestamibi	1.80 ± 0.20 (1.61–2.01)
^{99m}Tc–Teboroxime	2.02 ± 0.25 (1.78–2.30)
^{99m}Tc–3Fboroxime	2.41 ± 0.25 (2.15–2.65)
^{99m}Tc–5Fboroxime	2.50 ± 0.15 (2.28–2.62)
^{99m}Tc–MPYboroxime	2.41 ± 0.25 (2.15–2.65)
^{99m}Tc–PMboroxime	2.11 ± 0.15 (2.11–2.51)

[a]Range obtained from three animals.

ime and ^{99m}Tc–PMboroxime. All new ^{99m}Tc(III) radiotracers shared very similar 2 min heart uptake, which follows the general ranking order of ^{99m}Tc–5Fboroxime ~ ^{99m}Tc–MPYboroxime > ^{99m}Tc–PMboroxime ~ ^{99m}Tc–3Fboroxime. ^{99m}Tc–5Fboroxime and ^{99m}Tc–MPYboroxime had the 2 min heart uptake higher than that reported for ^{99m}Tc–Teboroxime (3.00 ± 0.37%ID/g).[35] The 2 min blood radioactivity was almost identical for new radiotracers (Table 3). Because of their fast blood clearance, they all had relatively high 2 min heart-to-blood ratios (H/B = 7–8). They also had low muscle uptake with high heart-to-muscle ratios (H/M = 7–25). Among the new ^{99m}Tc(III) radiotracers evaluated in this study, ^{99m}Tc–5Fboroxime and ^{99m}Tc–MPYboroxime shared the highest 2 min heart uptake value. ^{99m}Tc–PMboroxime had the lowest uptake in the lungs. Considering the 2 min heart uptake, myocardial washout kinetics and heart-to-background ratios, ^{99m}Tc–5Fboroxime was selected for full-scale biodistribution to determine its heart uptake values at different time points (2, 5, 15, 30, and 60 min p.i.) and compare its heart washout kinetics with that of ^{99m}Tc–Teboroxime over the 60 min period.

Myocardial Washout Kinetics of ^{99m}Tc–5Fboroxime. Table 5 lists biodistribution data for ^{99m}Tc–5Fboroxime in SD rats at 5, 15, 30, and 60 min p.i. Figure 3 compares myocardial washout kinetics of ^{99m}Tc–5Fboroxime and ^{99m}Tc–Teboroxime. The heart uptake values for ^{99m}Tc–Teboroxime were from our previous report.[35] We found that the myocardial washout curves were best fit with the biexponential decay equation for both ^{99m}Tc–Teboroxime ($y = 0.53 + 0.78e^{-0.584X} + 2.26e^{-0.064X}$: $R^2 = 0.9985$) and ^{99m}Tc–5Fboroxime ($y = 0.95 + 1.37e^{-0.389X} + 2.68e^{-0.029X}$: $R^2 = 0.9700$). According to these equations, the initial heart uptake (at t = 0 min) was calculated to be 3.6% ID/g for ^{99m}Tc–Teboroxime and 5.0% ID/g for ^{99m}Tc–5Fboroxime. The % ID/g heart uptake values of ^{99m}Tc–5Fboroxime were much higher ($p < 0.01$) than those of ^{99m}Tc–Teboroxime over the 60 min period. The AUC value of ^{99m}Tc–5Fboroxime was almost twice of that for ^{99m}Tc–Teboroxime at 0–60 min p.i. The heart uptake of ^{99m}Tc–5Fboroxime was almost unchanged over the first 5 min after its administration, and its 15 min heart uptake was comparable to that of ^{99m}Tc–Teboroxime,[35] within the experimental error. It took ~5 min for ^{99m}Tc–5Fboroxime to approach the 1 min heart uptake value and ~9.5 min to reach the 2 min heart uptake value (Figure 3: ~ 3% ID/g) of ^{99m}Tc–Teboroxime. Because ^{99m}Tc–Teboroxime had a linear relationship between its heart uptake and the regional myocardial blood flow (0–5 mL/min/g) at 1–2 min after administration,[15] it is conceivable that ^{99m}Tc–5Fboroxime might have a similar linear uptake–flow relationship over the first 10 min after its administration, which should be long enough to obtain high-quality images of the heart using ^{99m}Tc–5Fboroxime as the radiotracer with either the standard or CZT-based ultrafast cardiac SPECT cameras. ^{99m}Tc–5Fboroxime has significant advantages over ^{99m}Tc–Teboroxime with respect to both the initial heart uptake and myocardial retention time.

Excretion Kinetics from Normal Organs. Figure 4 compares the uptake values in normal organs and heart-to-background ratios of ^{99m}Tc–5Fboroxime with those of ^{99m}Tc–Teboroxime. The radioactivity in blood, liver, lungs, and muscle are important because it has significant impact on the image contrast for heart imaging agents. In general, ^{99m}Tc–5Fboroxime shared a similar uptake with ^{99m}Tc–Teboroxime in the blood and muscles. The heart-to-blood and heart-to-muscle ratios of ^{99m}Tc–5Fboroxime were significantly higher than those of ^{99m}Tc–Teboroxime due to its higher heart uptake over the 60 min study period (Figure 4). Even though ^{99m}Tc–5Fboroxime had higher liver uptake than ^{99m}Tc–Teboroxime, they shared similar heart-to-liver ratios due to its high heart uptake. ^{99m}Tc–5Fboroxime and ^{99m}Tc–Teboroxime shared similar uptake in lungs; however, the heart-to-lung ratios of ^{99m}Tc–5Fboroxime were significantly higher than those of ^{99m}Tc–Teboroxime at 5 and 30 min p.i. In addition, ^{99m}Tc–5Fboroxime had relatively low radioactivity in blood vessels (0.63–0.73% ID/g) around the coronary arteries. This observation is consistent with the lower radioactivity accumulation above the heart in planar images of the SD rats administered with ^{99m}Tc–5Fboroxime (Figure 2). Similar results were also obtained with ^{99m}Tc–PAboroxime and ^{99m}Tc–ISboroxime.[36]

DOI: 10.1021/acs.bioconjchem.6b00552
Bioconjugate Chem. 2016, 27, 2770–2779

Table 4. Selected Biodistribution Data (2 min) for ^{99m}Tc−3Fboroxime, ^{99m}Tc−5Fboroxime, ^{99m}Tc−MPYboroxime, and ^{99m}Tc−PMboroxime in SD Rats (n = 3)

radiotracer	^{99m}Tc−3Fboroxime	^{99m}Tc−5Fboroxime	^{99m}Tc−MPYboroxime	^{99m}Tc−PMboroxime
blood	0.41 ± 0.02	0.49 ± 0.05	0.65 ± 0.33	0.42 ± 0.03
brain	0.13 ± 0.03	0.08 ± 0.01	0.06 ± 0.01	0.10 ± 0.00
fat[a]	0.26 ± 0.10	0.35 ± 0.09	0.31 ± 0.05	0.43 ± 0.01
heart	3.25 ± 0.77	3.75 ± 0.15	3.73 ± 0.24	3.47 ± 0.15
intestines	1.18 ± 0.22	1.20 ± 0.08	0.83 ± 0.16	1.38 ± 0.02
kidneys	3.61 ± 0.73	3.85 ± 0.48	3.76 ± 0.66	3.23 ± 0.18
liver	4.40 ± 0.52	4.23 ± 0.57	3.40 ± 0.90	3.45 ± 0.16
lungs	2.28 ± 0.47	3.86 ± 1.58	2.11 ± 1.20	1.56 ± 0.31
muscle	0.16 ± 0.04	0.15 ± 0.03	0.17 ± 0.06	0.18 ± 0.05
spleen	1.69 ± 0.29	1.52 ± 0.28	1.83 ± 0.40	1.46 ± 0.02
vessels[b]	0.65 ± 0.04	0.73 ± 0.28	0.75 ± 0.26	0.94 ± 0.09
heart-to-blood ratio	8.07 ± 2.16	7.78 ± 0.53	6.89 ± 3.55	8.20 ± 0.16
heart-to-liver ratio	0.74 ± 0.12	0.90 ± 0.09	1.17 ± 0.39	1.01 ± 0.09
heart-to-lung ratio	1.33 ± 0.58	1.11 ± 0.33	2.19 ± 1.13	2.30 ± 0.37
heart-to-muscle ratio	20.68 ± 3.58	25.64 ± 4.45	24.71 ± 8.99	21.45 ± 5.54

[a]Fatty tissue around the heart. [b]Coronary artery and blood vessels above the heart.

Table 5. Selected Biodistribution Data (% ID/g) for ^{99m}Tc−5Fboroxime in SD Rats (200−220 g) at 5, 15, 30, and 60 min Post-injection

organ	5 min (n = 4)	15 min (n = 3)	30 min (n = 3)	60 min (n = 4)
blood	0.48 ± 0.08	0.28 ± 0.01	0.25 ± 0.01	0.23 ± 0.04
brain	0.08 ± 0.01	0.05 ± 0.01	0.07 ± 0.02	0.06 ± 0.01
fat[a]	0.45 ± 0.04	0.31 ± 0.01	0.25 ± 0.03	0.21 ± 0.07
heart	3.91 ± 0.09	2.83 ± 0.08	2.04 ± 0.14	1.43 ± 0.21
intestines	1.46 ± 0.23	2.10 ± 0.51	1.14 ± 0.29	1.84 ± 0.45
kidneys	3.43 ± 0.47	2.20 ± 0.05	1.64 ± 0.17	2.15 ± 1.16
liver	4.34 ± 0.92	4.42 ± 0.58	2.51 ± 0.10	2.57 ± 0.87
lungs	2.03 ± 0.42	1.10 ± 0.14	1.22 ± 0.40	1.27 ± 0.58
muscle	0.35 ± 0.18	0.18 ± 0.05	0.20 ± 0.03	0.17 ± 0.02
spleen	1.59 ± 0.08	0.83 ± 0.06	0.79 ± 0.10	0.64 ± 0.21
vessels	0.45 ± 0.13	0.73 ± 0.17	0.67 ± 0.01	0.47 ± 0.31
heart-to-blood ratio	8.44 ± 1.50	9.97 ± 0.19	8.07 ± 0.87	6.20 ± 0.41
heart-to-liver ratio	0.87 ± 0.27	0.65 ± 0.09	0.81 ± 0.03	0.59 ± 0.10
heart-to-lung ratio	2.01 ± 0.41	2.59 ± 0.19	1.89 ± 0.67	1.43 ± 0.70
heart-to-muscle ratio	14.03 ± 5.57	16.71 ± 3.57	10.67 ± 1.62	8.43 ± 1.53

[a]Fat tissues around blood vessels on the heart.

SPECT Imaging in SD Rats. Figure 5 shows the 3D, coronal, sagittal and transaxial views of SPECT images from the SD rats administered with ^{99m}Tc−5Fboroxime at 0−5 min p.i. Both right and left ventricular walls were clearly delineated. The interference from liver radioactivity in coronal and transaxial images was not significant. In the sagittal views, the liver radioactivity overlapped significantly with that in the inferior wall of the heart (Figures 5 and S2). Figure 6 displays the selected coronal views of SPECT images for the SD rats administered with ^{99m}Tc−5Fboroxime and ^{99m}Tc−Teboroxime at 0−5, 5−10, 10−15, 15−20, 20−25, and 25−30 min p.i. The best SPECT image acquisition window is 0−5 min for ^{99m}Tc−5Fboroxime due to its high initial uptake (Table 3). Longer acquisition time did not improve the image quality most likely due to its high liver uptake. High-quality SPECT images of the rat hearts were acquired using ^{99m}Tc−5Fboroxime in any of the 5 min window over the first 20 min after injection (Figure 6). In contrast, the myocardial washout of ^{99m}Tc−Teboroxime was too fast to obtain high-quality heart images at >5 min p.i. These results are consistent with those from planar imaging studies (Figure 2). The combination of high initial heart uptake with long myocardial retention time makes it possible to use ^{99m}Tc−5Fboroxime as the radiotracer for MPI studies with both standard and CZT-based cardiac SPECT cameras.

DISCUSSION

An ideal perfusion radiotracer should have a high heart uptake with a relatively stable myocardial retention, which linearly tracks the regional blood flow over a wide range flow rates. Stable myocardial retention is important because the rapid decrease in the heart uptake often leads to changes in myocardial extraction fraction and loss of the linear relationship. For example, the linear relationship between the heart uptake of ^{99m}Tc−Teboroxime and the regional myocardial blood flow rate (1−5 mL/m/g) was well-maintained at 1−2 min after injection.[19] However, its heart uptake underestimates the flow changes at high or moderate flow rates ~5 min after injection due to the "roll-off" phenomena,[3,20−25] which leads to a progressive loss of linearity when the regional blood flow is >3.0 mL/m/g.[15] Thus, the new radiotracer must have the heart uptake close to that of ^{99m}Tc−Teboroxime (3.0−3.5%ID/g at 1−2 min p.i. in the SD rats) to maintain the linear relationship

DOI: 10.1021/acs.bioconjchem.6b00552
Bioconjugate Chem. 2016, 27, 2770−2779

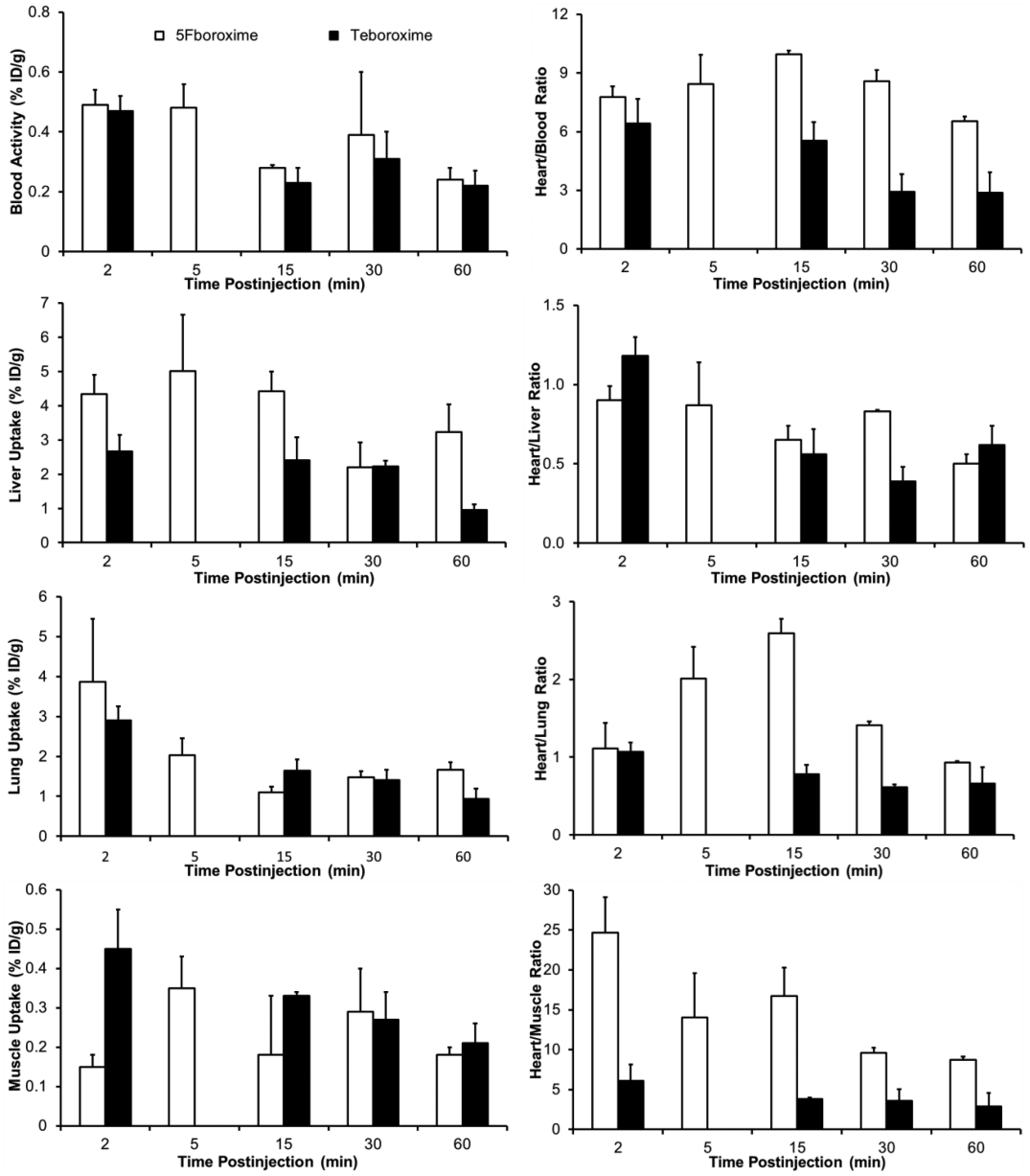

Figure 4. Comparison of organ uptake and heart-to-background ratios between ^{99m}Tc−5Fboroxime and ^{99m}Tc−Teboroxime.

between its myocardial uptake and the blood flow rate. It is difficult to quantify the myocardial radioactivity without this linear relationship.

In this study, we found that the boronate caps have significant impact on both initial heart uptake and myocardial washout kinetics of ^{99m}Tc(III) radiotracers [^{99m}TcCl(CDO)-$(CDOH)_2$B−R]. For example, ^{99m}Tc−HPboroxime is the most hydrophilic radiotracer with the HPLC retention time of 7.2 min (Table 1) due to the hydroxyl group on the pyridine ring, and its heart uptake is the lowest. In contrast, ^{99m}Tc−3Fboroxime is the most lipophilic radiotracer with the HPLC retention time of 16.5 min (Table 1), and its 2 min heart uptake is slightly lower than that of ^{99m}Tc−5Fboroxime (Table 4). ^{99m}Tc−5Fboroxime and ^{99m}Tc−MPYboroxime share a similar 2 min heart uptake (Table 4), but the AUC value for ^{99m}Tc−5Fboroxime is significantly higher than that for ^{99m}Tc−MPYboroxime (Table 2). Among the ^{99m}Tc(III) radiotracers evaluated in this study, ^{99m}Tc−5Fboroxime has the highest AUC value over the 60 min study period. The heart uptake of ^{99m}Tc−5Fboroxime is significantly higher than that reported for ^{99m}Tc−Teboroxime and ^{99m}Tc−PAboroxime.[35,36] In addition, ^{99m}Tc−5Fboroxime is able to maintain its heart uptake above 3.5% ID/g for >5 min and more than 3.0% ID/g for ∼10 min (Figure 3). High-quality SPECT images of the rat hearts could be acquired using ^{99m}Tc−5Fboroxime in any of the 5 min image acquisition window over the first 20 min after administration (Figure 6). Therefore, ^{99m}Tc−5Fboroxime is better than ^{99m}Tc−Teboroxime as a radiotracer for SPECT MPI. Unlike ^{99m}Tc−Sestamibi and ^{99m}Tc−Tetrofosmin, the heart localization of which depends on the negative mitochondrial potential,[40,41] ^{99m}Tc−5Fboroxime and ^{99m}Tc−Teboroxime are true perfusion radiotracers because their biodistribution properties are largely weighted by blood flow instead of receptor-binding or metabolism. Development of such a radiotracer is of great value for accurate quantification of the regional myocardial blood flow with the stress MPI. The

DOI: 10.1021/acs.bioconjchem.6b00552
Bioconjugate Chem. 2016, 27, 2770−2779

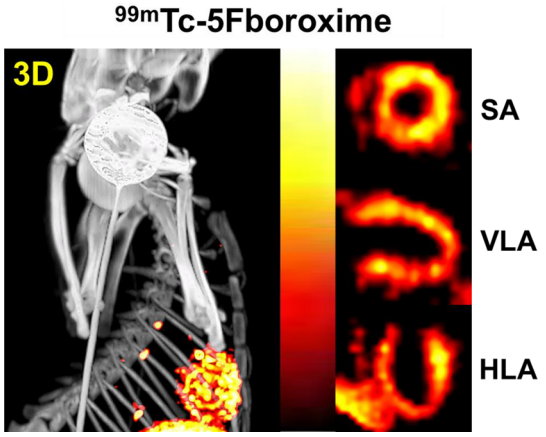

Figure 5. Selected 3D, coronal, sagittal, and transaxial views of SPECT images of the SD rat administered with ~150 MBq of ^{99m}Tc−5Fboroxime at 0−5 min p.i. SA = short axis; VLA = vertical long axis; HLA = horizontal long axis. SPECT images were obtained with the camera being focused in the heart region using a u-SPECT-II scanner. Anesthesia was induced using an air-flow rate of 350 mL/min and ~3.0% isoflurane.

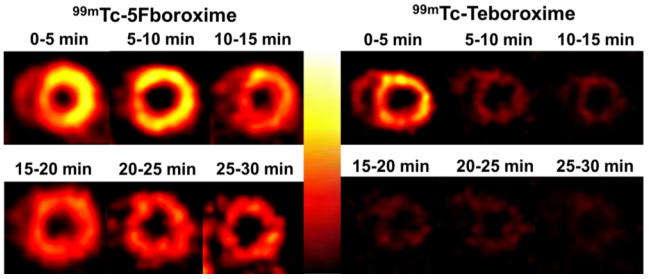

Figure 6. Selected coronal views of SPECT images of the SD rats administered with ~150 MBq of ^{99m}Tc−5Fboroxime and ^{99m}Tc−Teboroxime at 0−5, 5−10, 10−15, 15−20, 20−25, and 25−30 min post-injection. ^{99m}Tc−Teboroxime was used for comparison purpose. High-quality SPECT images were acquired using ^{99m}Tc−5Fboroxime in any of the 5 min windows over the first 20 min. The heart washout of ^{99m}Tc−Teboroxime was too fast to obtain high-quality images at >5 min post-injection.

fact that >90% perfusion procedures are currently performed with SPECT in nuclear cardiology further illustrates the clinical significance of developing new ^{99m}Tc perfusion radiotracers.

The key question is why ^{99m}Tc−5Fboroxime has higher heart uptake with myocardial retention time significantly longer than ^{99m}Tc−Teboroxime. One possible explanation is related to higher in vivo Tc−Cl bond stability. It was reported that complex [^{99m}TcCl(CDO)$(CDOH)_2$B−R] tends to be more stable in vivo when the R group contains two or more carbon atoms.[12,42] In this study, we found that ^{99m}Tc−5Fboroxime was stable both in the kit matrix (with excess NaCl) and in the diluted solution containing 20−30% propylene glycol in saline. A more stable Tc−Cl bond makes it difficult for [^{99m}TcCl-(CDO)$(CDOH)_2$B−R] to convert into its "hydrolyzed form" [^{99m}Tc(OH)(CDO)$(CDOH)_2$B−R], which tends to have much lower first-pass extraction and less heart uptake than [^{99m}TcCl(CDO)$(CDOH)_2$B−R] does.[12,42]

Previously, we used the fast-phase half-life, which indicates the rate of heart radioactivity change, to evaluate the myocardial retention of ^{99m}Tc(III) radiotracers because their myocardial washout curves were all fitted the bi-exponential equation.[12,35−37] In this study, we found that the AUC value is a much better indicator than the fast-phase half-life. Longer myocardial retention time does not necessarily indicate a better radiotracer if its initial heart uptake is low. In contrast, the AUC value represents a combination of initial heart uptake and myocardial retention and is directly proportional to the total heart radioactivity of the radiotracer. A larger AUC value indicates more radioactivity accumulation in the heart during that specific period of time. For example, ^{99m}Tc−HPboroxime had the longer myocardial time than ^{99m}Tc−5Fboroxime, but its initial heart uptake (Table 2: 3.21 ± 0.68%ID) was significantly ($p < 0.01$) lower than that of ^{99m}Tc−5Fboroxime (Table 2: 5.10 ± 0.86%ID). As a result, the AUC value of ^{99m}Tc−5Fboroxime (Table 2: 129 ± 6) was more than twice of that for ^{99m}Tc−HPboroxime (Table 2: 62 ± 14). Therefore, the AUC values are better suited than the fast-phase half-lives for evaluation of new ^{99m}Tc radiotracers.

It is important to note that the heart uptake values obtained from dynamic planar imaging (Table 2) are significantly different from those from biodistribution (Tables 3−5) due to the method of planar imaging. The radioactivity from planar image quantification is accumulative over a specific period of imaging time, and the heart uptake from biodistribution is obtained at a specific time point. The heart uptake values from planar image quantification include parts of radioactivity in the blood pool and surrounding normal organs. Although the heart uptake values can be corrected by deducting the normal organ radioactivity, it is impossible to separate the blood-pool radioactivity from that in the myocardium. In fact, the high initial heart uptake obtained from planar image quantification is most likely caused by the presence of blood radioactivity for radiotracers [^{99m}TcCl(CDO)$(CDOH)_2$B−R] (Table 2). Dynamic planar imaging is useful as a frontline screening tool to evaluate myocardial washout kinetics of ^{99m}Tc radiotracers without sacrificing a large number of animals, but the tissue γ-counting remains the most accurate method to determine biodistribution properties of new ^{99m}Tc radiotracers.

A significant drawback with ^{99m}Tc−5Fboroxime is its higher liver uptake than that of ^{99m}Tc−Teboroxime (Figure 5), but its heart-to-liver ratios compare well with those of ^{99m}Tc−Teboroxime within the experimental error of biodistribution assay (Figure 5). The intense liver radioactivity may interfere with the visualization of inferior wall using standard dual-head SPECT cameras currently available in nuclear cardiology. However, this drawback can be overcome using the CZT-based ultrafast cardiac SPECT cameras (such as D-SPECT). In this situation, the patient can be placed in the upright position during image acquisition. As a result, there is a better separation between the cardiac and hepatic radioactivity because the liver tends to drop more downward than does the heart in this position, leading to the reduced interference from the liver radioactivity.

CONCLUSIONS

Boronate caps have significant impact on the heart uptake and myocardial washout kinetics of radiotracers [^{99m}TcCl(CDO)-$(CDOH)_2$B−R]. Among the new ^{99m}Tc radiotracers evaluated in this study, ^{99m}Tc−5Fboroxime shows higher initial heart uptake and longer myocardial retention than ^{99m}Tc−Teboroxime. ^{99m}Tc−5Fboroxime has better heart-to-blood, heart-to-lung, and heart-to-muscle ratios than ^{99m}Tc−Teboroxime over the 60 min period. The combination of its high heart uptake and long myocardial retention makes it possible to image the

DOI: 10.1021/acs.bioconjchem.6b00552
Bioconjugate Chem. 2016, 27, 2770−2779

heart using ^{99m}Tc−5Fboroxime as the radiotracer with both standard and CZT-based ultrafast cardiac SPECT cameras.

EXPERIMENTAL METHODS

Materials. Chemicals (citric acid, γ-cyclodextrin, cyclohexanedione dioxime (CDOH), diethylenetriaminepentaacetic acid (DTPA), 2-formylfuran-5-boronic acid (5F), furan-3-boronic acid (3F), 6-hydroxylpyridine-2-boronic acid (HP), 5-methoxypyridine-3-boronic acid (MPY), pyridine-4-boronic acid (4PY), 1,5-pyrimidine-3-boronic acid (PM), sodium chloride, and $SnCl_2{\cdot}2H_2O$) were purchased from Sigma-Aldrich (St. Louis, MO) and were used without further purification. $Na^{99m}TcO_4$ were obtained from Cardinal HealthCare (Chicago, IL).

Radio-HPLC Method. The radio high-performance liquid chromatography (radio-HPLC) method used an Agilent HP-1100 HPLC system (Agilent Technologies, Santa Clara, CA) equipped with a β-ram IN/US detector (Tampa, FL) and Zorbax C_8 column (4.6 mm × 250 mm, 300 Å pore size; Agilent Technologies, Santa Clara, CA). The flow rate was 1 mL/min. The mobile phase was isocratic with 30% solvent A (10 mM NH_4OAc buffer, pH = 6.8) and 70% solvent B (methanol) between 0 and 5 min, followed by a gradient from 70% solvent B at 5 min to and 90% solvent B at 15 min and an isocratic mobile phase with 10% solvent A and 90% solvent B. The RCP was reported as the percentage of area for the expected radiometric peak on each radio-HPLC chromatogram of ^{99m}Tc radiotracer. The ITLC method used Gelman Sciences silica gel strips and a 1:1 (v:v) mixture of acetone and saline as the mobile phase. ^{99m}Tc radiotracers and $^{99m}TcO_4^-$ migrated to the solvent front, and the [^{99m}Tc]colloid stayed at the origin.

Preparation of [^{99m}TcCl(CDO)(CDOH)$_2$B−R]. Complexes [^{99m}TcCl(CDO)(CDOH)$_2$B−R] (R = 2F, 3F, 5F, HP, MPY, PM, and 4PY) were prepared using the kit formulation.[36−38] Each lyophilized vial contains 2 mg of $CDOH_2$, 4−5 mg of boronic acid, 50 μg of $SnCl_2{\cdot}2H_2O$, 9 mg of citric acid, 2 mg of DTPA, 20 mg of NaCl, and 20 mg of γ-cyclodextrin. A total of 1.0 mL of $^{99m}TcO_4^-$ solution (370−1110 MBq) was added to a lyophilized vial. The vial was then heated at 100 °C for 10−15 min. A sample of the resulting solution was diluted with saline containing ∼20% propylene glycol to 3.7 MBq/mL. The diluted solution was analyzed by radio-HPLC and ITLC. The RCP was 95−98% with minimal amount of [^{99m}Tc]colloid (<0.5%).

Solution Stability. The new radiotracer was first prepared using the procedure above. The solution stability of a specific radiotracer was monitored by radio-HPLC at 0, 2, 4, and 6 h post-labeling. For the solution stability in diluted solution, a sample of the radiotracer kit solution was diluted with saline containing 20−30% propylene glycol to 3.7 MBq/mL. The diluted solution was analyzed by radio-HPLC at 0 and 6 h after dilution.

Doses Preparation. Doses for biodistribution were prepared by dissolving radiotracer kit solution to ∼1.1 MBq/mL with saline containing 20% propylene glycol. Doses for imaging studies were made by dissolving the ^{99m}Tc radiotracer solution to ∼370 MBq/mL with saline containing 20% propylene glycol. All dose solutions were filtered with a 0.20 μm filter unit to eliminate foreign particles before being injected into animals. The injection volume was ∼0.1 mL per animal for biodistribution and 0.2−0.5 mL per animal for imaging studies.

Animal Preparation. Animal studies were conducted in compliance with the NIH animal experiment guidelines (Principles of Laboratory Animal Care, NIH Publication nos. 86−23, revised 1985). The protocols for biodistribution and imaging studies were approved by the Purdue University Animal Care and Use Committee (PACUC). The SD rats (200−250 g) were purchased from Harlan (Indianapolis, IN) and were acclimated for >24 h. Animals were anesthetized with intramuscular injection of a mixture of ketamine (80 mg/kg) and xylazine (19 mg/kg) before being used for biodistribution and planar imaging studies.

Protocol for Biodistribution. A total of 12 SD rats (200−250 g) were divided into three groups. Each animal was administered with 100−111 KBq of ^{99m}Tc radiotracer via tail vein injection. A total of four animals were sacrificed by sodium pentobarbital overdose (100−200 mg/kg) at 2, 15, and 30 min p.i. Blood was withdrawn from the heart. Organs of interest (heart, brain, intestines, kidneys, liver, lungs, muscle, and spleen) were harvested, rinsed with saline, dried with absorbent tissues, weighed, and counted for radioactivity on a PerkinElmer Wizard −1480 γ-counter (Shelton, CT). The organ uptake was reported as the percentage of injected dose per gram of organ tissue (% ID/g). A comparison between two radiotracers was made using one-way ANOVA test (GraphPad Prim 5.0, San Diego, CA). The level of significance was set at $p < 0.05$.

Protocol for Planar Imaging in SD Rats. Dynamic imaging studies were performed in SD rats (n = 5; 200−250 g). Each animal was administered with ^{99m}Tc radiotracer (40−80 MBq) via tail vein injection. Once ^{99m}Tc radiotracer was administered, the animal was immediately placed prone on a single head mini γ-camera (Diagnostic Services Inc., NJ). The 1 min images were acquired during first 5 min p.i., followed by 2 min images at 6−30, 40, 50, and 60 min p.i. The imaging data were stored digitally in a 128 × 128 matrix. After imaging, animals were returned to a lead-shielded cage. Because new radiotracers had little via hepatobiliary and renal routes, planar images were analyzed by drawing regions of the heart (the heart radioactivity) and whole body (the injected dose into each animal). The background was corrected by drawing the region above heart. The results were expressed as the percentage of injected radioactivity (% ID). The curve fit of heart washout kinetics was determined using GraphPad Prim 5.0 (GraphPad Software, Inc., San Diego, CA). The data were reported as an average ± standard deviation based on the results from between four and six animals at each time point. A comparison between two radiotracers was made using a one-way ANOVA test. The level of significance was set at $p < 0.05$.

Protocol for SPECT in SD Rats. SPECT imaging was performed the u-SPECT-II/CT scanner (Milabs, Utrecht, The Netherlands) equipped with a 1.0 mm multipinhole collimator. The SD rat was placed into a shielded chamber connected to an isoflurane anesthesia unit (Univentor, Zejtun, Malta). Anesthesia was induced using an air flow rate of 350 mL/min and ∼3.0% isoflurane and maintained using an air flow of ∼250 mL/min with ∼2.5% isoflurane during image data acquisition (6 frames, 75 projections over 5 min per frame). The animal was administered with ^{99m}Tc−5Fboroxime (∼150 MBq) in 0.5 mL of saline containing ∼20% propylene glycol. Rectangular scan in regions of interest (ROIs) from SPECT and CT were selected one the basis of orthogonal X-ray images provided by the CT. After SPECT acquisition, the animal was allowed to recover in a shielded cage.

DOI: 10.1021/acs.bioconjchem.6b00552
Bioconjugate Chem. 2016, 27, 2770−2779

Image Reconstruction and Data Processing. SPECT reconstruction was performed using a POSEM (pixelated ordered subsets by expectation maximization) algorithm with 6 iterations and 16 subsets. CT data were reconstructed using a cone-beam filtered back-projection algorithm (NRecon v1.6.3, Skyscan). After reconstruction, the SPECT and CT data were automatically coregistered according to the movement of the robotic stage, and resampled to equivalent voxel sizes. Co-registered images were further rendered and visualized using the PMOD software (PMOD Technologies, Zurich, Switzerland). A 3D Gaussian filter (1.2 mm full width half maximum) was applied to smooth noise, and the lookup tables were adjusted for good visual contrast. The images were visualized as both orthogonal slices and maximum intensity projections.

■ ASSOCIATED CONTENT

Supporting Information

The Supporting Information is available free of charge on the ACS Publications website at DOI: 10.1021/acs.bioconjchem.6b00552.

Figures showing radio-HPLC chromatograms of new ^{99m}Tc radiotracers and the coronal, sagittal and transaxial views of SPECT images of the SD rats. (PDF)

■ AUTHOR INFORMATION

Corresponding Authors

*W.F. e-mail: nuclearfw@126.com.

*S.L. e-mail: liu100@purdue.edu.

Notes

The authors declare no competing financial interest.

■ ACKNOWLEDGMENTS

This work was supported, in part, by Purdue University, the grant R21 EB017237-01 (S.L.) from the National Institute of Biomedical Imaging and Bioengineering (NIBIB), and a grant 81401446 from the National Nature Science Foundation of China (Y.Z.).

■ ABBREVIATIONS USED

AUC, area under the curve; CAD, coronary artery disease; CT, computed tomography; CZT, cadmium−zinc−telluride; DTPA, diethylenetriaminepentaacetic acid; ITLC, instant thin-layer chromatography; MPI, myocardial perfusion imaging; RCP, radiochemical purity; SPECT, single photon-emission computed tomography; ^{18}F-BMS747158−02, 2-*tert*-butyl-4-chloro-5-[4-(2-(^{18}F)fluoroethoxy-methyl)benzyloxy]-2*H*-pyridazin-3−1; ^{99m}Tc−2Fboroxime, [^{99m}TcCl(CDO)(CDOH)$_2$B−2F] (CDOH$_2$ = cyclohexanedione dioxime; 2F, 3-formylfuran-2-yl); ^{99m}Tc−3Fboroxime, [^{99m}TcCl(CDO)(CDOH)$_2$B−3F] (3F = furan-3-yl); ^{99m}Tc−5Fboroxime, [^{99m}TcCl(CDO)-(CDOH)$_2$B−5F] (5F = 2-formylfuran-5-yl); ^{99m}Tc−3PYboroxime, [^{99m}TcCl(CDO)(CDOH)$_2$B−3PY] (3PY = pyridin-3-yl); ^{99m}Tc−4PYboroxime, [^{99m}TcCl(CDO)(CDOH)$_2$B−4PY] (4PY = pyridin-4-yl); ^{99m}Tc−HPboroxime, [^{99m}TcCl(CDO)-(CDOH)$_2$B−HP] (HP = 2-hydroxylpyridin-5-yl); ^{99m}Tc−ISboroxime, [^{99m}TcCl(CDO)(CDOH)$_2$B−IS] (IS = isoxazol-4-yl); ^{99m}Tc−MPYboroxime, [^{99m}TcCl(CDO)(CDOH)$_2$B−MPY] (MPY = 3-methoxypyridin-5-yl); ^{99m}TcN−NOET, [^{99m}TcN(NOET)$_2$] (NOET = *N*-ethoxy,*N*-ethyl-(dithiocarbamato); ^{99m}Tc−PAboroxime, [^{99m}TcCl(CDO)-(CDOH)$_2$B(1*H*-pyrazol-3-yl)] (PA = 1*H*-pyrazol-3-yl); ^{99m}Tc−PMboroxime, [^{99m}TcCl(CDO)(CDOH)$_2$B−PM] (PM = pyrimidin-5-yl); ^{99m}Tc−Sestamibi, [^{99m}Tc(MIBI)$_6$]$^+$ (MIBI = 2-methoxy-2-methylpropylisonitrile); and ^{99m}Tc−Teboroxime, [^{99m}TcCl(CDO)(CDOH)$_2$B−Me]

■ REFERENCES

(1) Henneman, M. M., Schuijf, J. D., van der Wall, E. E., and Bax, J. J. (2006) Non-invasive anatomical and functional imaging for the detection of coronary artery disease. *Br. Med. Bull. 79*−*80*, 187−202.

(2) Di Carli, M. F., and Hachamovitch, R. (2007) New technology for noninvasive evaluation of coronary artery disease. *Circulation 115*, 1464−1480.

(3) Baggish, A. L., and Boucher, C. A. (2008) Radiopharmaceutical agents for myocardial perfusion imaging. *Circulation 118*, 1668−1674.

(4) Slomka, P. J., Patton, J. A., Berman, D. S., and Germano, G. (2009) Advances in technical aspects of myocardial perfusion SPECT imaging. *J. Nucl. Cardiol. 16*, 255−76.

(5) Salerno, M., and Beller, G. A. (2009) Noninvasive assessment of myocardial perfusion. *Circ.: Cardiovasc. Imaging 2*, 412−424.

(6) Stirrup, J., Wechalekar, K., Maenhout, A., and Anagnostopoulos, C. (2009) Cardiac radionuclide imaging in stable coronary artery disease and acute coronary syndromes. *Br. Med. Bull. 89*, 63−78.

(7) Slomka, P. J., Berman, D. S., and Germano, G. (2014) Absolute myocardial blood flow quantification with SPECT/CT: Is it possible? *J. Nucl. Cardiol. 21*, 1092−1095.

(8) Nekolla, S. G., Rischpler, C., and Nakajima, K. (2014) Myocardial blood flow quantification with SPECT and conventional tracers: a critical appraisal. *J. Nucl. Cardiol. 21*, 1089−1091.

(9) Henzlova, M., and Duvall, W. (2011) The future of SPECT MPI: Time and dose reduction. *J. Nucl. Cardiol. 18*, 580−587.

(10) Klein, R., Hung, G. U., Wu, T. C., Huang, W. S., Li, D., deKemp, R. A., and Hsu, B. (2014) Feasibility and operator variability of myocardial blood flow and reserve measurements with ^{99m}Tc-sestamibi quantitative dynamic SPECT/CT imaging. *J. Nucl. Cardiol. 21*, 1075−1088.

(11) Narra, R. K., Nunn, A. D., Kuczynski, B. L., Feld, T., Wedeking, P., and Eckelman, W. C. (1989) A neutral technetium-99m complex for myocardial imaging. *J. Nucl. Med. 30*, 1830−1837.

(12) Rumsey, W. L., Rosenspire, K. C., and Nunn, A. D. (1992) Myocardial extraction of teboroxime: effects of teboroxime interaction with blood. *J. Nucl. Med. 33*, 94−101.

(13) Marshall, R. C., Leidholdt, E. M., Jr., Zhang, D. Y., and Barnett, C. A. (1991) The effect of flow on technetium-99m-teboroxime (SQ30217) and thallium-201 extraction and retention in rabbit heart. *J. Nucl. Med. 32*, 1979−1988.

(14) Leppo, J. A., and Meerdink, D. J. (1990) Comparative myocardial extraction of two technetium-labeled BATO derivatives (SQ30217, SQ32014) and thallium. *J. Nucl. Med. 31*, 67−74.

(15) Beanlands, R., Muzik, O., Nguyen, N., Petry, N., and Schwaiger, M. (1992) The relationship between myocardial retention of technetium-99m teboroxime and myocardial blood flow. *J. Am. Coll. Cardiol. 20*, 712−719.

(16) Johnson, L. L. (1994) Myocardial perfusion imaging with technetium-99m-teboroxime. *J. Nucl. Med. 35*, 689−692.

(17) Iskandrian, A. S., Heo, J., Nguyen, T., and Mercuro, J. (1991) Myocardial imaging with Tc-99m teboroxime: technique and initial results. *Am. Heart J. 121*, 889−894.

(18) Esteves, F. P., Raggi, P., Folks, R. D., Keidar, Z., Askew, J. W., Rispler, S., O'Connor, M. K., Verdes, L., and Garcia, E. V. (2009) Novel solid-state-detector dedicated cardiac camera for fast myocardial perfusion imaging: multicenter comparison with standard dual detector cameras. *J. Nucl. Cardiol. 16*, 927−934.

(19) Buechel, R. R., Pazhenkottil, A. P., Herzog, B. A., Husmann, L., Nkoulou, R. N., Burger, I. A., Valenta, I., Wyss, C. A., Ghadri, J. R., and Kaufmann, P. A. (2010) Real-time breath-hold triggering of myocardial perfusion imaging with a novel cadmium-zinc-telluride detector gamma camera. *Eur. J. Nucl. Med. Mol. Imaging 37*, 1903−1908.

DOI: 10.1021/acs.bioconjchem.6b00552
Bioconjugate Chem. 2016, 27, 2770−2779

(20) Duvall, W. L., Croft, L. B., Godiwala, T., Ginsberg, E., George, T., and Henzlova, M. J. (2010) Reduced isotope dose with rapid SPECT MPI imaging: initial experience with a CZT SPECT camera. *J. Nucl. Cardiol. 17*, 1009−1014.
(21) Schillaci, O., and Danieli, R. (2010) Dedicated cardiac cameras: a new option for nuclear myocardial perfusion imaging. *Eur. J. Nucl. Med. Mol. Imaging 37*, 1706−1709.
(22) Fiechter, M., Ghadri, J. R., Kuest, S. M., Pazhenkottil, A. P., Wolfrum, M., Nkoulou, R. N., Goetti, R., Gaemperli, O., and Kaufmann, P. A. (2011) Nuclear myocardial perfusion imaging with a novel cadmium-zinc-telluride detector SPECT/CT device: first validation versus invasive coronary angiography. *Eur. J. Nucl. Med. Mol. Imaging 38*, 2025−2030.
(23) Gimelli, A., Bottai, M., Genovesi, D., Giorgetti, A., Di Martino, F., and Marzullo, P. (2012) High diagnostic accuracy of low-dose gated-SPECT with solid-state ultrafast detectors: Preliminary clinical results. *Eur. J. Nucl. Med. Mol. Imaging 39*, 83−90.
(24) Imbert, L., Poussier, S., Franken, P. R., Songy, B., Verger, A., Morel, O., Wolf, D., Noel, A., Karcher, G., and Marie, P. Y. (2012) Compared performance of high-sensitivity cameras dedicated to myocardial perfusion SPECT: A comprehensive analysis of phantom and human images. *J. Nucl. Med. 53*, 1897−1903.
(25) Nakazato, R., Berman, D. S., Hayes, S. M., Fish, M., Padgett, R., Xu, Y., Lemley, M., Baavour, R., Roth, N., and Slomka, P. J. (2013) Myocardial perfusion imaging with a solid state camera: Simulation of a very low dose imaging protocol. *J. Nucl. Med. 54*, 373−379.
(26) Ben-Haim, S., Murthy, V. L., Breault, C., Allie, R., Sitek, A., Roth, N., Fantony, J., Moore, S. C., Park, M. A., Kijewski, M., et al. (2013) Quantification of myocardial perfusion reserve using dynamic SPECT imaging in humans: A feasibility study. *J. Nucl. Med. 54*, 873−879.
(27) Mouden, M., Ottervanger, J. P., Knollema, S., Timmer, J. R., Reiffers, S., Oostdijk, A. H. J., de Boer, M. J., and Jager, P. L. (2014) Myocardial perfusion imaging with a cadmium zinc telluride-based gamma camera versus invasive fractional flow reserve. *Eur. J. Nucl. Med. Mol. Imaging 41*, 956−962.
(28) van Dijk, J. D., Jager, P. L., Mouden, M., Slump, C. H., Ottervanger, J. P., de Boer, J., Oostdijk, A. H. J., and van Dalen, J. A. (2014) Development and validation of a patient-tailored dose regime in myocardial perfusion imaging using CZT-SPECT. *J. Nucl. Cardiol. 21*, 1158−1167.
(29) Wells, R. G., Timmins, R., Klein, R., Lockwood, J., Marvin, B., deKemp, R. A., Wei, L., and Ruddy, T. D. (2014) Dynamic SPECT measurement of absolute myocardial blood flow in a porcine model. *J. Nucl. Med. 55*, 1685−1691.
(30) Cerqueira, M. D., Garcia, E. V., Gropler, r R. J., and Udelson, J. E. (2007) Eighth Nuclear Cardiology Invitational Conference Park City, Utah, 2006. *J. Nucl. Cardiol. 14*, e15−e25.
(31) Ward, R. P., Al-Mallah, M. H., Grossman, G. B., Hansen, C. L., Hendel, R. C., Kerwin, T. C., McCallister, B. D., Jr., Mehta, R., Polk, D. M., Tilkemeier, P. L., et al. (2007) American Society of Nuclear Cardiology review of the ACCF/ASNC appropriateness criteria for single-photon emission computed tomography myocardial perfusion imaging (SPECT MPI). *J. Nucl. Cardiol. 14*, e26−e38.
(32) Garcia, E. V., and Gropler, R. J. (2008) Ninth nuclear cardiology invitational conference, Annapolis, Maryland, 2008. *J. Nucl. Cardiol. 15*, e37−e50.
(33) Bailey, D. L., and Willowson, K. P. (2013) An evidence-based review of quantitative SPECT imaging and potential clinical applications. *J. Nucl. Med. 54*, 83−89.
(34) Nekolla, S. G., Rischpler, C., and Nakajima, K. (2014) Myocardial blood flow quantification with SPECT and conventional tracers: a critical appraisal. *J. Nucl. Cardiol. 21*, 1089−1091.
(35) Zheng, Y., Ji, S., Tomaselli, E., Ernest, C., Freiji, T., and Liu, S. (2014) Effect of co-ligands on chemical and biological properties of ^{99m}Tc(III) complexes [^{99m}Tc(L) (CDO) $(CDOH)_2$BMe] (L = Cl, F, SCN and N_3; $CDOH_2$ = cyclohexanedione dioxime). *Nucl. Med. Biol. 41*, 813−824.
(36) Yang, Y., Zheng, Y., Tomaselli, E., Fang, W., and Liu, S. (2015) Impact of boronate-capping groups on biological characteristics of ^{99m}Tc(III) complexes [^{99m}TcCl(CDO) $(CDOH)_2$B-R] ($CDOH_2$ = cyclohexanedione dioxime). *Bioconjugate Chem. 26*, 316−328.
(37) Liu, M., Zheng, Y., Avcibasi, U., and Liu, S. (2016) Novel ^{99m}Tc(III)-azide complexes [^{99m}Tc(N_3) (CDO) $(CDOH)_2$B-R] ($CDOH_2$ = Cyclohexanedione Dioxime) as potential radiotracers for heart Imaging. *Nucl. Med. Biol. 43*, 732−741.
(38) Jurisson, S., Francesconi, L., Linder, K. E., Treher, E., Malley, M. F., Gougoutas, J. Z., and Nunn, A. D. (1991) Syntheses, characterization, and reactivity of manganese and rhenium dioxime complexes. X-ray crystal structures of Mn^{II}(CDO) $(CDOH)_2(BPh(OCH_3))_2$, an unusual pseudoclathrochelate complex, and Re^{III}CI(CDO) $(CDOH)_2$BPh. *Inorg. Chem. 30*, 1820−1827.
(39) Hsieh, W. Y., and Liu, S. (2006) Novel biscapped and monocapped tris(dioxime) Mn(II) complexes: X-ray crystal structure of the first cationic tris(dioxime) Mn(II) complex [Mn-$(CDOH)_3$BPh]OH ($CDOH_2$ = 1,2-cyclohexanedione dioxime). *Inorg. Chem. 45*, 5034−5043.
(40) Carvalho, P. A., Chiu, M. L., Kronauge, J. F., Kawamura, M., Jones, A. G., Holman, B. L., and Piwnica-Worms, D. (1992) Subcellular distribution and analysis of technetium-99m-MIBI in isolated perfused rat hearts. *J. Nucl. Med. 33*, 1516−1522.
(41) Younes, A., Songadele, J. A., Maublant, J., Platts, E., Pickett, R., and Veyre, A. (1995) Mechanism of uptake of technetium-tetrofosmin II: uptake into isolated adult rat heart mitochondria. *J. Nucl. Cardiol. 2*, 327−333.
(42) Jurisson, S. S., Hirth, W., Linder, K. E., Di Rocco, R. J., Narra, R. K., Nowotnik, D. P., and Nunn, A. D. (1991) Chloro→hydroxy substitution on technetium BATO [TcCl(dioxime)$_3$BR] complexes. *Int. J. Rad. Appl. Instrum. B 18*, 735−744.

DOI: 10.1021/acs.bioconjchem.6b00552
Bioconjugate Chem. 2016, 27, 2770−2779